

## THERMAL BARRIER COATING LIFE PREDICTION MODEL DEVELOPMENT\*

J. T. DeMasi and Dr. K. D. Sheffler  
United Technologies Corporation  
Pratt & Whitney

The objective of this program is to establish a methodology to predict Thermal Barrier Coating (TBC) life on gas turbine engine components. The approach involves experimental life measurement coupled with analytical modeling of relevant degradation modes. The coating being studied is a flight qualified two layer system, designated PWA 264, consisting of a nominal ten mil layer of seven percent yttria partially stabilized zirconia plasma deposited over a nominal five mil layer of low pressure plasma deposited NiCoCrAlY. Thermal barrier coating degradation modes being investigated include: thermomechanical fatigue, oxidation, erosion, hot corrosion, and foreign object damage.

The program is divided into two phases; the first phase, currently in progress, has identified cyclic mechanical damage to the ceramic and interfacial oxidation as the predominant degradation and failure modes (Task I) and is developing (Task II) and substantiating (Task III) a correlative life prediction model for these predominant modes. Phase II will address mechanistically based modeling for all relevant degradation modes.

## PHASE I, TASK I - FAILURE MECHANISM DETERMINATION

The objective of Task I was to identify predominant TBC failure modes and to develop a preliminary correlative life prediction model for these modes. The approach to failure mode identification included an extensive review of experimental and flight service hardware, together with a laboratory test program designed to study the influence of driving forces such as temperature, frequency, transients, environment, coating thickness, etc. on degradation and failure life.

Results of the hardware evaluation indicate the predominant failure mode to be thermomechanical spallation of the ceramic coating layer, resulting from the formation of a dominant ceramic crack parallel and closely adjacent to the metal-ceramic interface as shown in figure 1.

Laboratory burner rig and furnace exposure test results show cyclic coating life to be reduced by increased temperature, increased coating thickness, reduced cycle rate, pre-induced oxidation damage, and artificial sea salt injected into the burner flame. Analysis of these data leads to the conclusion that cyclic mechanical damage to the ceramic and interfacial oxidation of the underlying metal layer are the predominant degradation modes in clean fuel cyclic thermal exposure. Exposure to salt contamination more severe than that normally encountered in commercial flight service can cause premature ceramic failure.

Metallographic examination of specimens removed from the burner rig test at various fractions of expected spallation life shows ceramic cracking as early as 20% of expected life. Examination of crack morphology at successively increasing life

\*Work conducted under NASA Contract NAS3-23944

fractions suggests that spallation results from progressive link-up of adjacent subcritical cracks as opposed to subcritical growth of a single dominant crack as presented in figure 2. Direct evidence of interfacial initiated cracking is difficult to find, indicating that the role of oxidation in damage accumulation may be less direct than previously thought. It is interesting to note that examples of scale initiated cracking are easier to find in older specimens, occurring in the same structure together with larger numbers of well developed longer cracks which appear to be isolated from the interface. This observation could suggest that the thicker oxide scale developed at longer exposure times can initiate cracks, but that this is not the "critical" damage mode in the sense that those cracks which propagate to failure are initiated early in life and appear to be isolated from the interface. An example of this is found in figure 3.

To support the Task I preliminary modeling effort, mechanical property tests were conducted on bulk ceramic fabricated by plasma deposition with a structure that closely simulates the strain tolerant ceramic coating. The most significant result of these tests is the observation of highly non-linear tensile stress-strain behavior at all temperatures between ambient and 2200°F. This data is summarized in figure 4. While there is significant variability of initial and overall stiffness, the basic non-linear shape of the stress-strain curve is similar at temperatures up to 2000°F. At 2200°F there is substantially more curvature than at lower temperatures. Both ultimate tensile strength and tensile failure strain are relatively low ( $\approx 3\text{Ksi}$  and  $\approx 0.3\%$ ) at all temperatures.

Compressive stress-strain behavior, summarized in figure 5, differs significantly from tensile behavior; compressive strengths are much higher than tensile strengths, and there appears to be distinct linear and non-linear segments to the stress-strain curves. The 1000°F and 1600°F compressive stress-strain curves clearly are shaped differently than corresponding tensile stress-strain curves. At 2200°F, compressive deformation begins to resemble tensile deformation. Initial compressive stiffness appears to be essentially independent of temperature in the range studied.

As shown in figures 6 and 7, the strain tolerant ceramic exhibits a significant creep response at 1800°F and 2200°F; no response was observed in a tensile creep test conducted at 1000°F. Based on this observation, it will be important to incorporate a time dependent material response in the advanced modeling effort.

The data plotted in figure 8 shows an apparently real fatigue response in the strain tolerant ceramic, but with a stress dependence substantially different from that observed in metals. Whereas metallic materials typically exhibit slopes ranging from  $\approx -1.5$  with reversed plasticity to  $\approx -8$  in the fully elastic range, the data in figure 8 appears to have a slope on the order of  $-50$ . Specific degradation and failure mechanisms responsible for this very stress sensitive fatigue behavior are not presently understood.

Preliminary fracture toughness tests indicate that toughness for cracking perpendicular to the splat structure is on the order of  $0.5 \text{ Ksi} \sqrt{\text{in}}$ ; it is expected that toughness for in-plane cracking, where predominant failure cracks are located in the coating, would be even lower.

#### PHASE I, TASK I PRELIMINARY LIFE PREDICTION MODEL DEVELOPMENT

The preliminary life prediction model focuses on the two major damage modes identified in the laboratory testing described above. The first of these modes in-

volves a mechanical driving force, resulting from cyclic strains and stresses in the ceramic layer caused by thermally induced and externally imposed loads. The second is an environmental driving force which appears, based on the experimental results, to be related to "oxidation damage", due to the in-service growth of a NiCoCrAlY oxide scale at the metal-ceramic interface. Based on the apparently "mechanical" mode of ceramic failure (near interfacial ceramic cracking), and on the difficulty in finding metallographic evidence of a direct physical link between the growing oxide scale and incipient cracking in specimens exposed to a relatively small fraction of expected life, it was elected to follow the approach of Miller (ref. 1) and employ an existing phenomenological fatigue model (Manson - Coffin) as the basis for the TBC life model. In traditional form, this model relates cyclic inelastic strain range to a number of cycles to fatigue failure. To incorporate an environmental effect, the mechanical driver is analytically modified in such a way as to reduce the apparent fatigue strength of the ceramic layer. The use of inelastic strain range as a damage driver for the ceramic coating layer is considered justified in view of the previously mentioned nonlinearity observed in constitutive tests conducted on the strain tolerant ceramic material, including the observation of an open hysteresis loop in preliminary tests with reversed loading.

The mathematical form of the model is:  $(\Delta\epsilon_i / \Delta\epsilon_f)^b = N_f$

where  $\Delta\epsilon_i$  = Total cyclic inelastic strain range  
 $\Delta\epsilon_f$  = Failure strain  
 $N_f$  = Number of cycles to failure  
 $b$  = Constant

The total cyclic inelastic strain,  $\Delta\epsilon_i$ , is the sum of the  $\Delta(\alpha\Delta T)$  strain plus the heatup and cooldown strains,  $\Delta\epsilon_c$  and  $\Delta\epsilon_H$  respectively, due to the initial heatup and cooldown transient part of the burner rig thermal cycle:

$$\Delta\epsilon_i = \Delta(\alpha\Delta T) + \Delta\epsilon_c + \Delta\epsilon_H - 2(\sigma_{y.s.}/E)$$

The failure strain,  $\Delta\epsilon_f$ , is a function of the inelastic strain and is reduced by the strain due to the oxide thickness ratio,  $\delta / \delta_c$ , where  $\delta_c$  is the critical oxide thickness which will cause ceramic failure in a single thermal cycle:

$$\Delta\epsilon_f = \Delta\epsilon_{f_0} (1 - \delta / \delta_c)^c + \Delta\epsilon_i (\delta / \delta_c)^d$$

The static failure strain  $\Delta\epsilon_{f_0}$ , is the strain required to fail the ceramic in the absence of bond coat oxidation; c and d are "adjustable" constants set equal to unity in the preliminary analysis. Results achieved using this model to correlate approximately one hundred individual burner rig test results obtained on Task I are shown in figure 9. Achievement of a correlation coefficient of almost 0.9 is considered quite a good fit for this preliminary attempt.

#### PHASE I, TASK I - PRELIMINARY MODEL VERIFICATION TESTING

To challenge the preliminary model, three burner rig verification tests were conducted using a single, internally cooled hollow specimen. This specimen permits exposure of the ceramic with a steady state through a thickness gradient to more closely simulate engine exposure of the coating, and also allows more precise instrumentation and control of the thermal environment. The hollow verification test specimen is twice the diameter of the previously utilized specimen, and rotates

about its own axis to assure circumferential temperature uniformity. These substantial changes from the Task IB experimental condition assured that the preliminary model was effectively challenged by the verification testing.

Comparisons between observed and predicted cyclic life, presented in figure 10 indicate the need for significant model refinement in Task II. While the model predicts the uncooled test result quite accurately, the two cooled test results are not well predicted. Refinement of the model to improve prediction capability currently is being performed in Task II, described below.

#### PHASE I, TASK II - MAJOR MODE LIFE PREDICTION MODEL DEVELOPMENT

The objective of this task is to improve the prediction capability of the preliminary model developed in Task I. The approach involves refinement of the analytical model as well as the generation of additional "design data" for model calibration, using the improved test method first employed for the Task IC verification tests.

Analytical enhancements involve improved modeling of the ceramic constitutive and time dependent behavior, incorporation of an improved oxidation model developed by Dr. Robert A. Miller (which has yet to be published but which has been related to Pratt & Whitney through private communications with NASA), and refinement of the finite element calculation of temperature and stress-strain distribution. In addition to the improved simulation of engine exposure conditions, the experimental program incorporates an expanded parameter envelope to cover a broader range of mechanical and oxidation forcing functions, as depicted in figure 11. A large portion of this test matrix has been completed and the data is being used to correlate a new life prediction model.

More accurate modeling of ceramic behavior, including nonlinear stress-strain characteristics, asymmetric tensile and compressive response, and time dependent inelastic deformation, is being accomplished using a time dependent constitutive model developed by Walker (ref. 2). An example of the application of this model to the 2200°F tension and compression data is shown in figure 12. These results show the tensile behavior to be well modeled by the Walker approach; predictive capability in compression is quite good up to  $\approx -1\%$  strain; beyond this point the prediction departs significantly from observed behavior. An example of a hysteresis loop calculated for a typical strain emphasis burner rig cycle is shown schematically in figure 12. There are two significant observations concerning the calculated behavior. First, compressive strain remains below the  $-1\%$  limit, beyond which the prediction capability of the model breaks down. Second, the model predicts a very open loop with a quite large reversed plastic strain range to drive ceramic fatigue damage. Prediction for all of the experimental burner rig cycles currently is being made with this model for incorporation into the improved life prediction system.

Oxidation experiments were conducted using the program's substrate - TBC system, at the NASA Lewis Research Center. Dr. Robert Miller used this data to develop a new more accurate oxidation model for the improved life prediction system. The recommended weight gain expression for the data showed that the oxide growth rate is not parabolic, but approximates  $t^{0.29}$ . This new oxide growth rate expression in terms of oxide thickness is being incorporated into the advanced life prediction model.

## PHASE I - TASK III - MODEL VERIFICATION

The objective of this task is to validate the model developed in Task II through a series of approved benchmark engine mission simulation tests. Experimental approaches to further improve the simulation capability of the test method (i.e., generate higher heat fluxes and larger through thickness gradients), and thus more effectively challenge the model, currently are being explored for incorporation in the Task III verification testing. Based on results of these tests, recommendations for further research or refinement required to arrive at a fully satisfactory engine life prediction methodology shall be made, if necessary.

### REFERENCE

1. Miller, R.A.; "Oxidation-Based Model for Thermal Barrier Coating Life". J. Am. Cer. Soc. Vol. 67 No. 8, 1984, pp. 517-521.
2. Walker, K.P.; "Research and Development Program for Nonlinear Structural Modeling with Advanced Time-Temperature Dependent Constitutive Relationships". NASA-CR 165533.

ORIGINAL PAGE IS  
OF POOR QUALITY



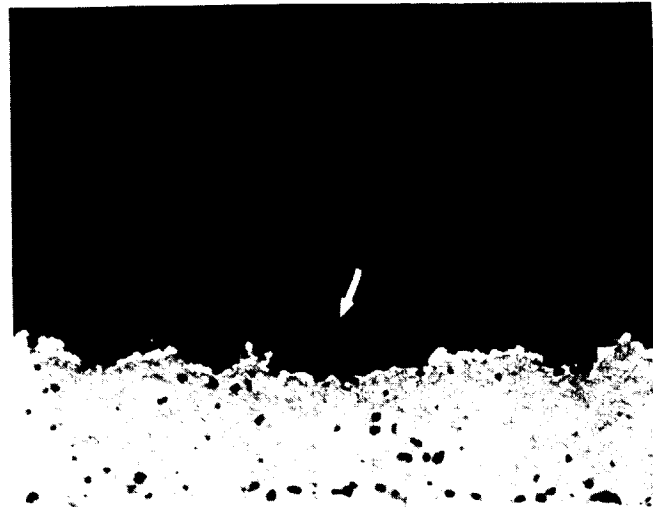
Figure 1 Typical Thermal Barrier Coating Engine Failure Mode

ORIGINAL PAGE IS  
OF POOR QUALITY



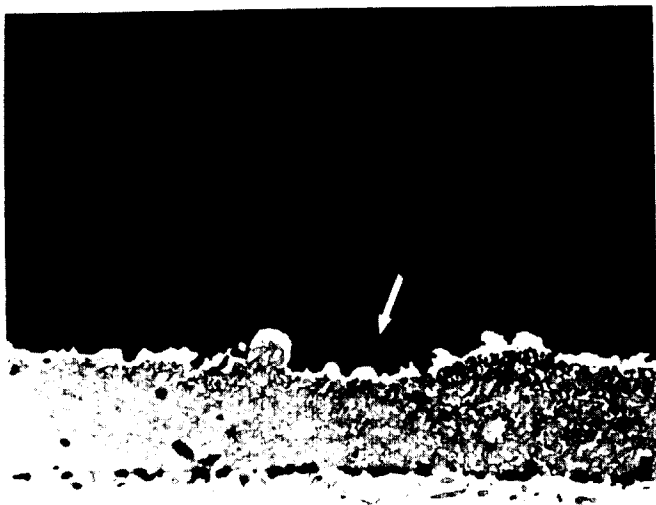
(a)

0%



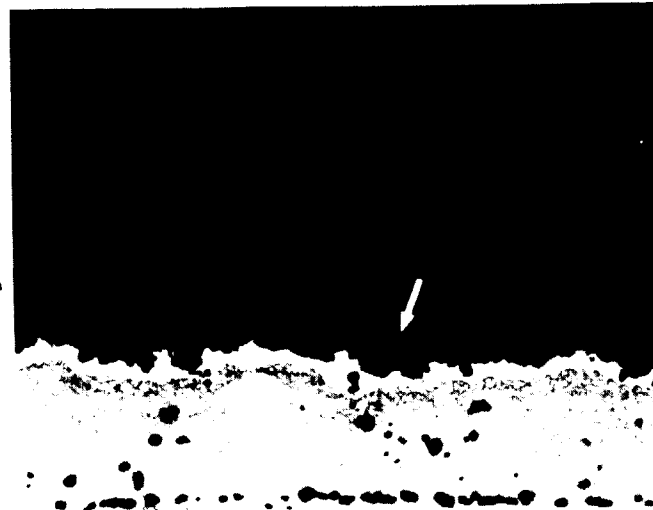
(b)

8.3% (15 hrs)



(c)

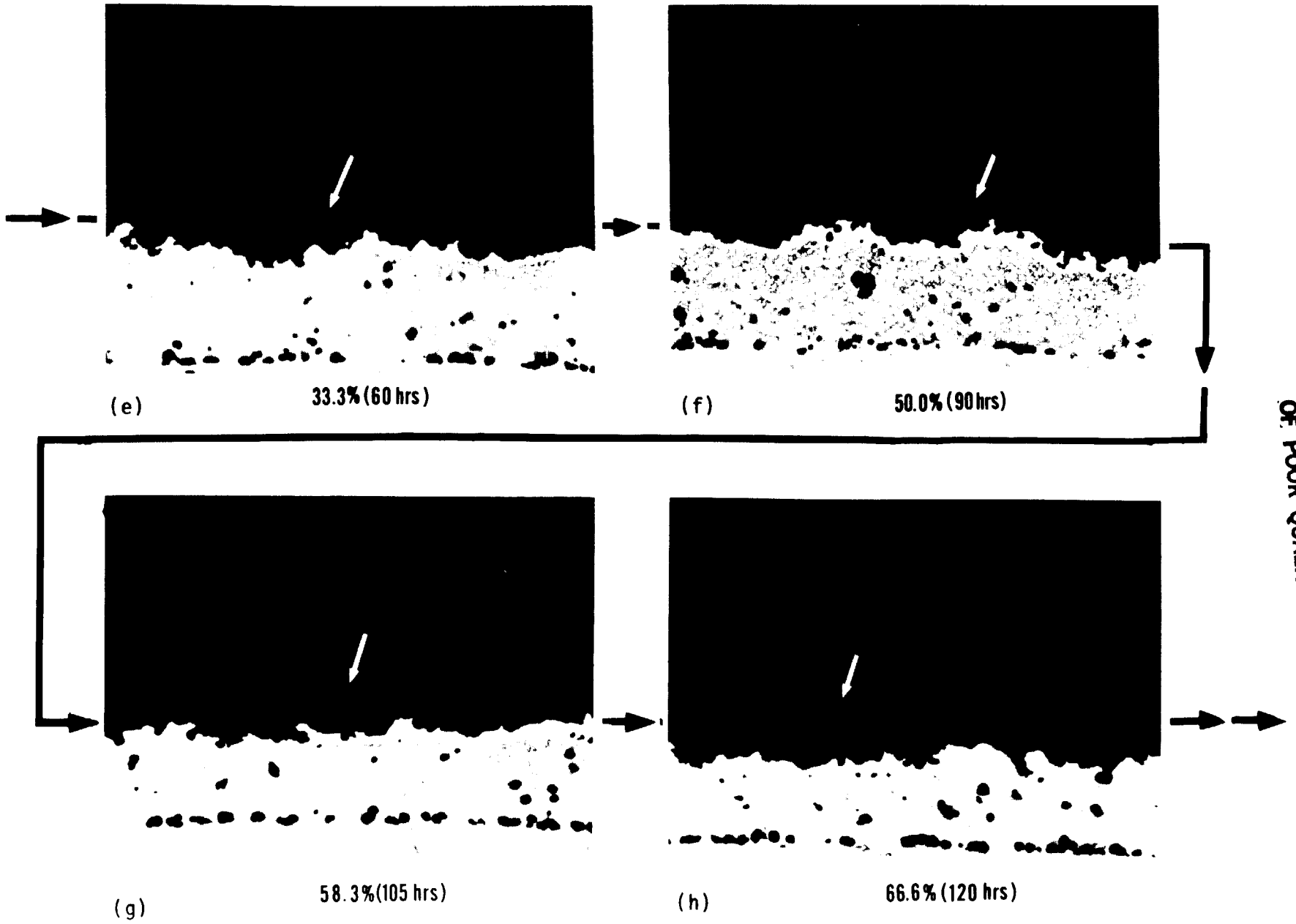
16.6% (30 hrs)



(d)

25.0% (45 hrs)

Figure 2 Thermal Barrier Coating Damage Progression



ORIGINAL PAGE IS  
OF POOR QUALITY

476

Figure 2 (Continued)



(i)

75.0% (135 hrs)



(j)

91.6% (165 hrs)

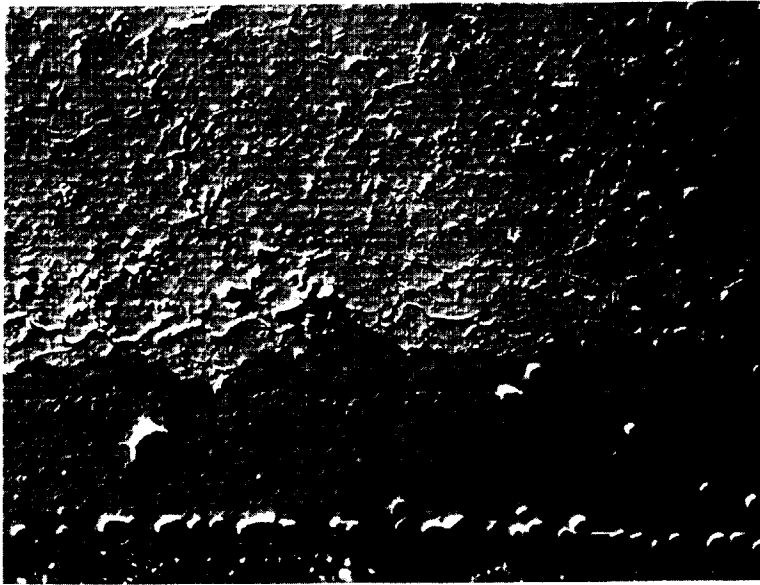


(k)

100% (180 hrs)

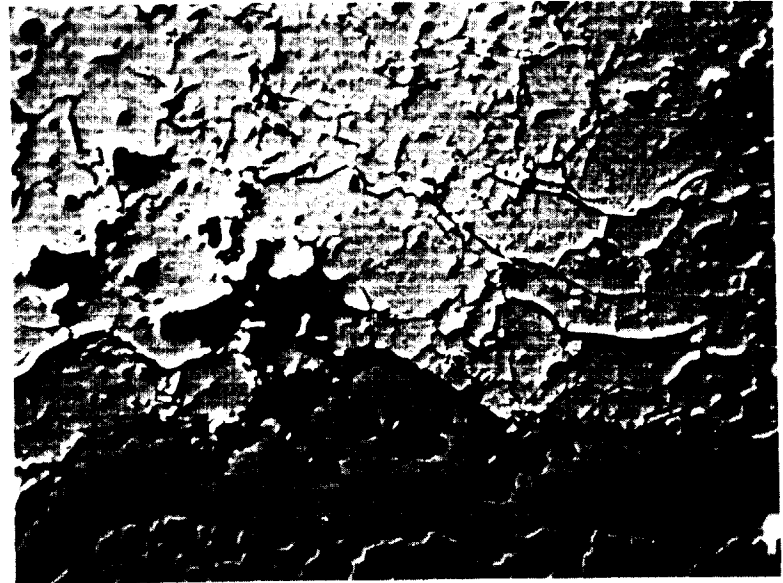
ORIGINAL PAGE IS  
OF POOR  
QUALITY

Figure 2 (Continued)



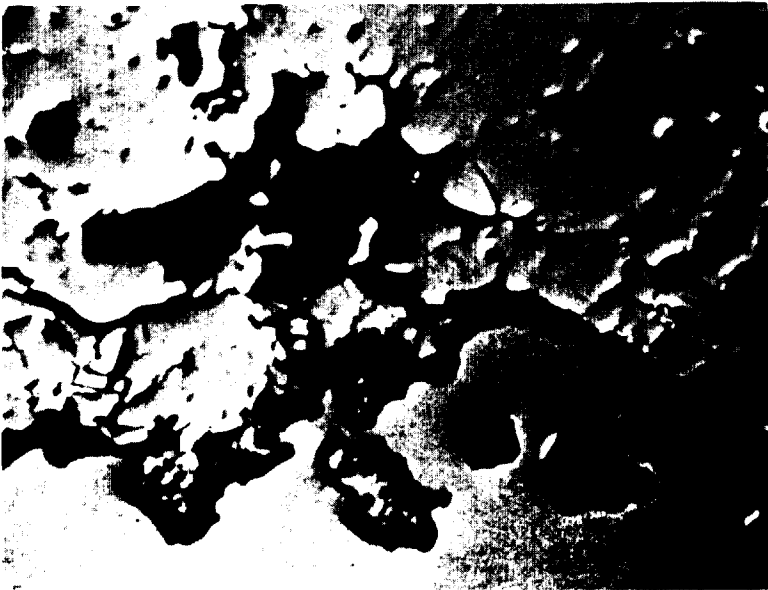
85-197

200X



85-197

500X



85-197

1000X



85-197

2000X

478

ORIGINAL PAGE IS  
OF POOR QUALITY

Figure 3 BSI of TBC After 105 Hours of Burner Rig Test Time at 2100°F/Short Cycle/Fast Heatup

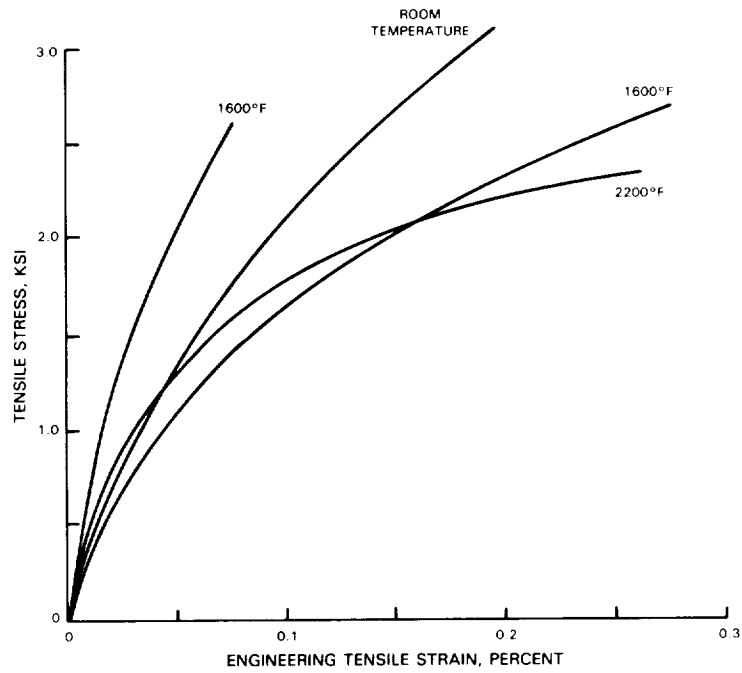


Figure 4 Representative Strain Tolerant Ceramic Tensile Stress Strain Curves at Various Temperatures. Room temperature strain data measured by strain gage; temperature curves obtained from corrected cross head displacement.

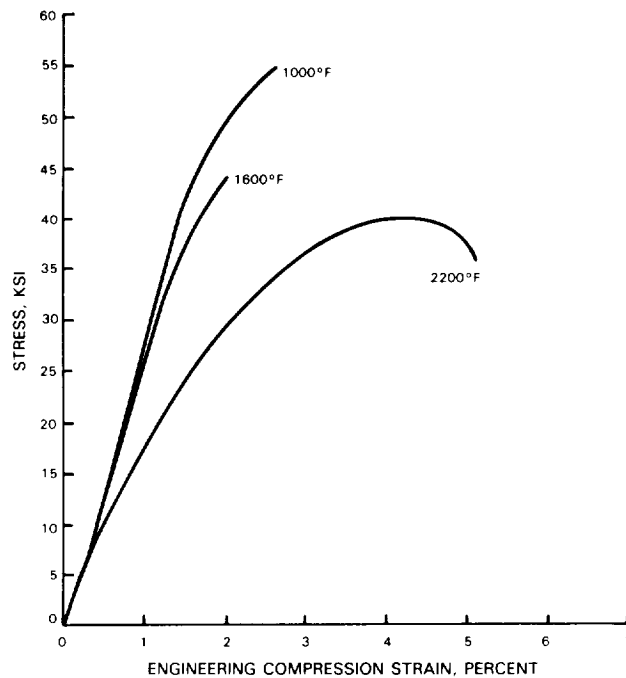


Figure 5 Representative Strain Tolerant Ceramic Compressive Stress-Strain Curves at Various Temperatures. Compressive strains calculated from corrected crosshead displacement.

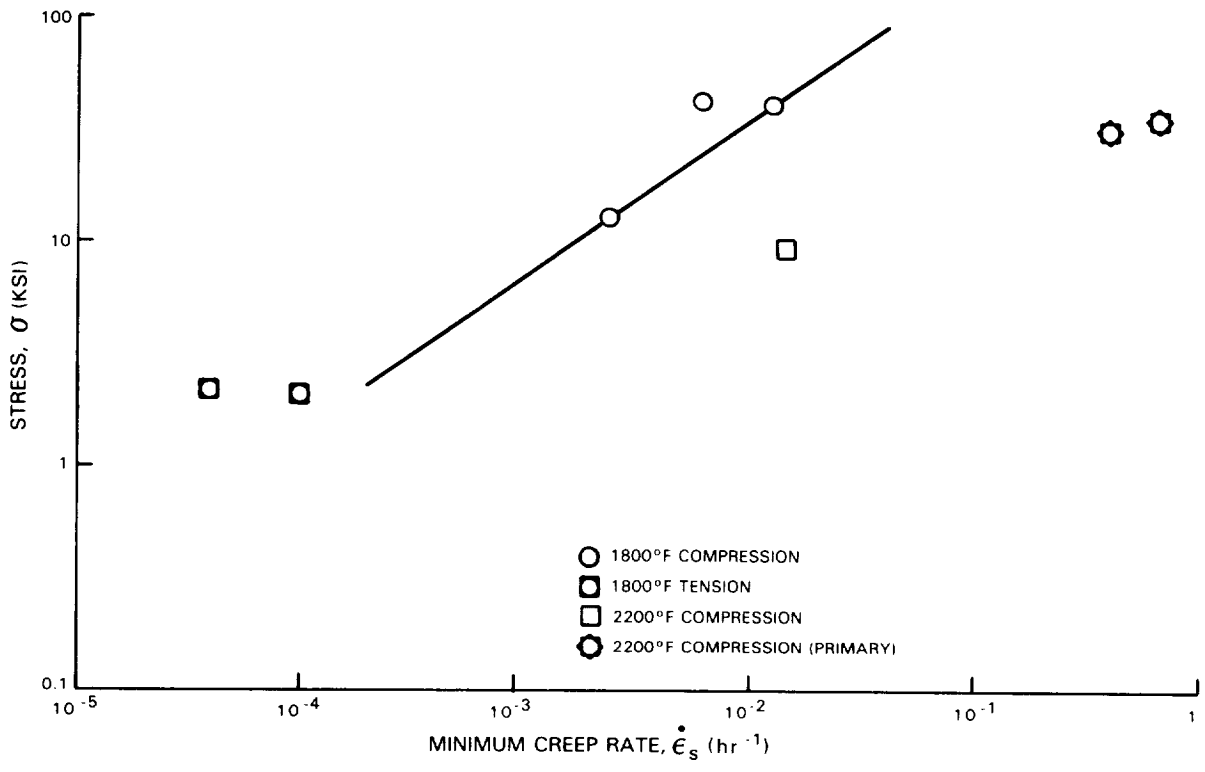


Figure 6 Stress Versus Creep Rate

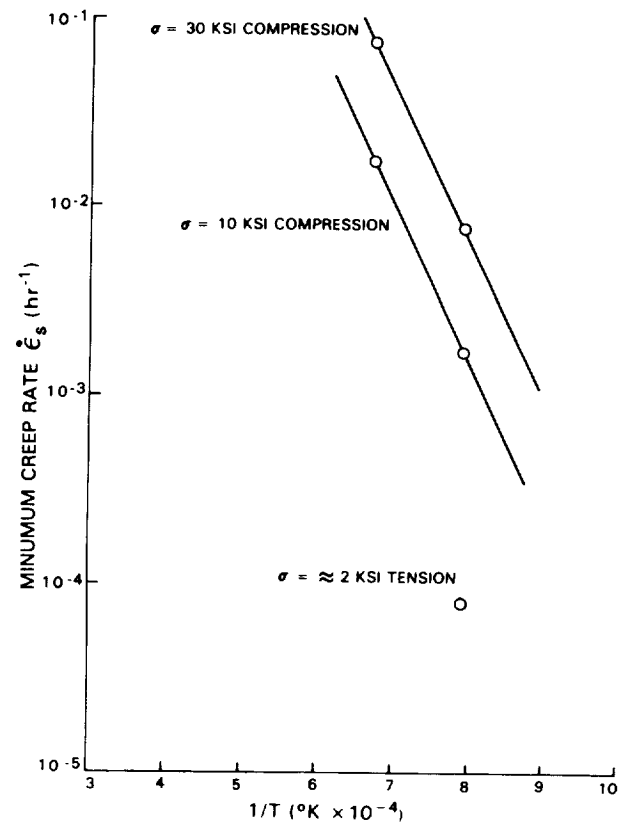


Figure 7 Creep Rate Versus Temperature

LOW CYCLE FATIGUE OF  
BULK PLASMA SPRAYED 7 w/o  $Y_2O_3 - ZrO_2$

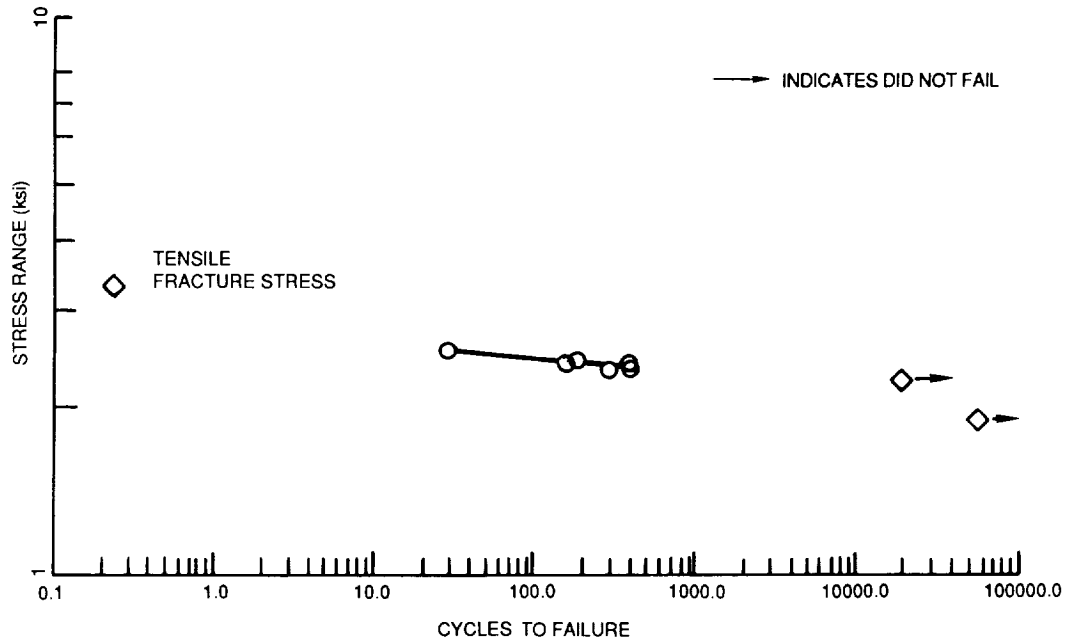


Figure 8 S-N Curve for 7YsZ (1000°F and 1600°F data plotted together)

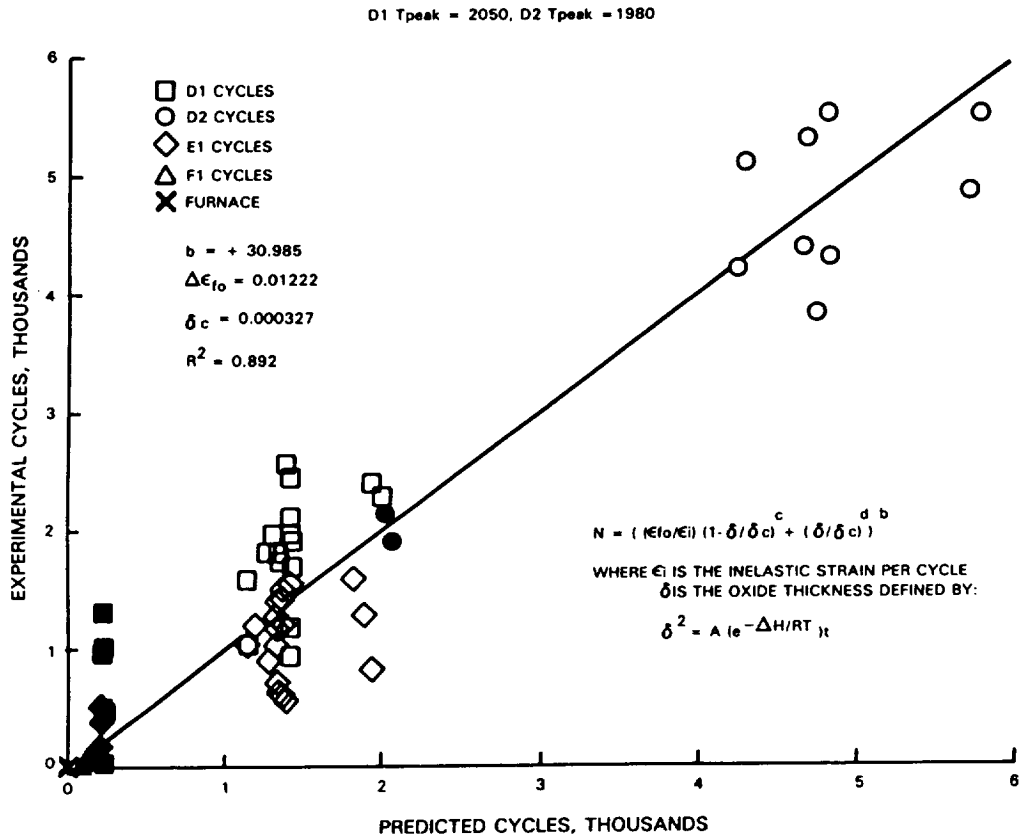


Figure 9 Preliminary Life Model Correlation

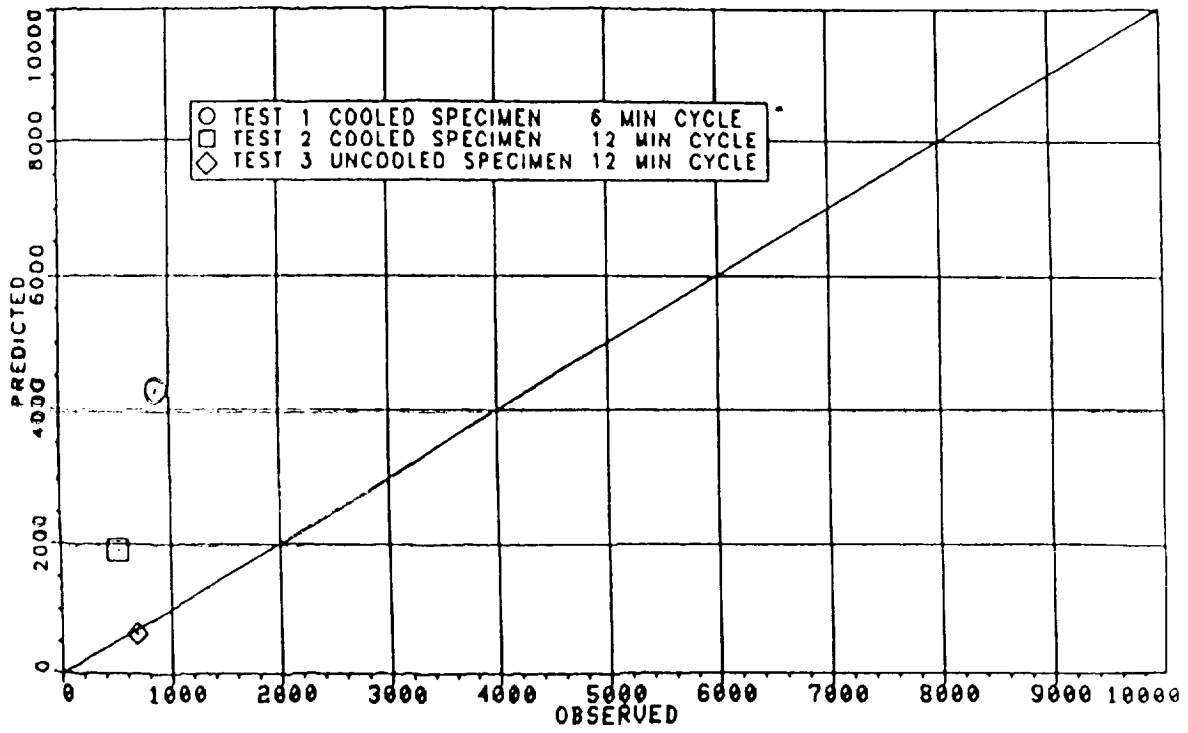


Figure 10 Predicted Cycles Versus Observed Cycles for the Task IC Verification Tests

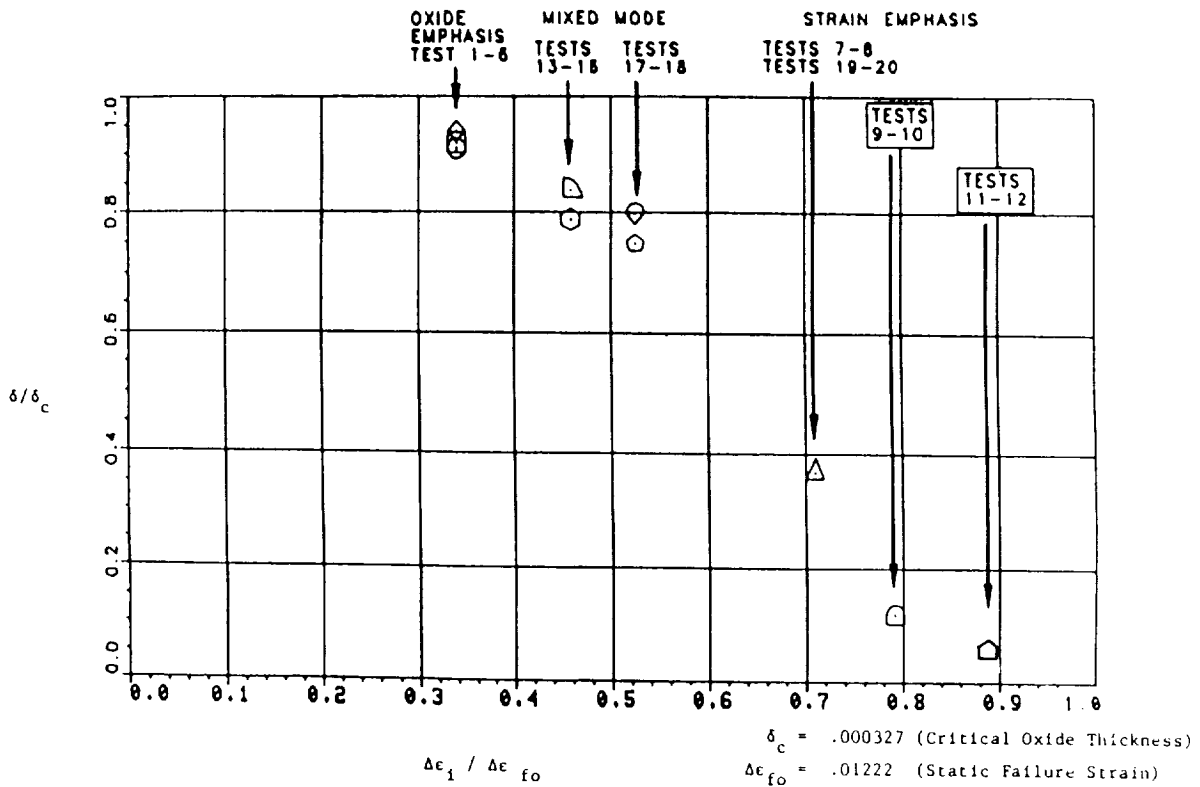


Figure 11 Task II Predictions; Oxide Thickness Ratio Versus Strain Ratio

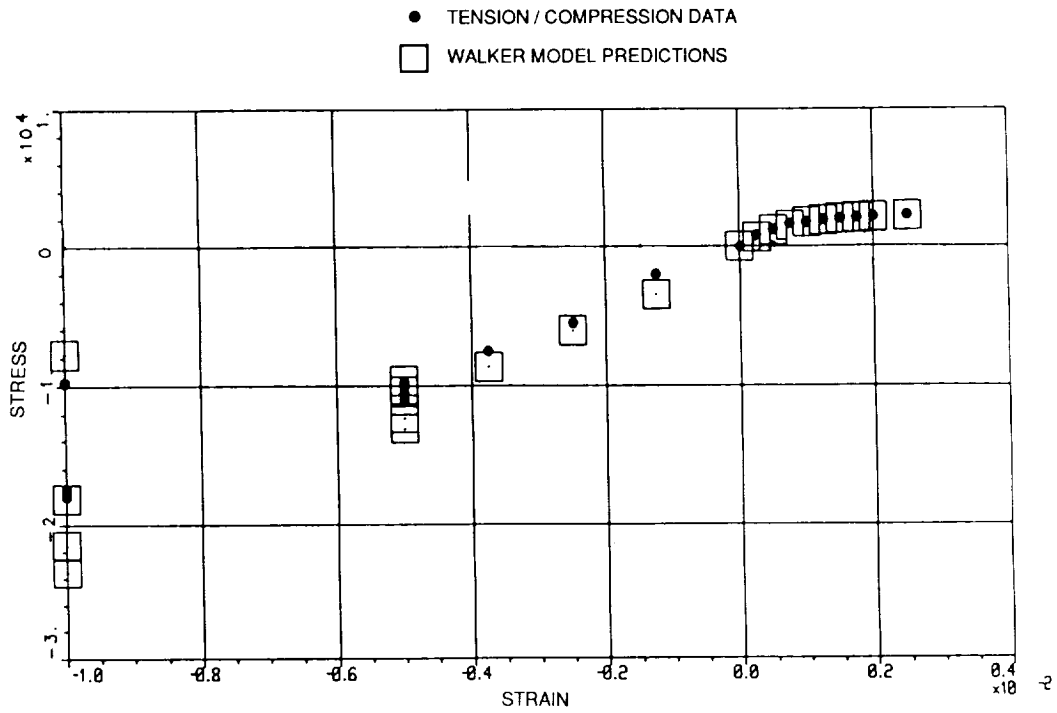


Figure 12 Compression and Tension Data at 2200°F Kevin Walker Model Predictions

- 1 INITIATION OF HEATING, TERMINATION OF COOLING
- 2 TERMINATION OF HEATING
- 3 INITIATION OF COOLING

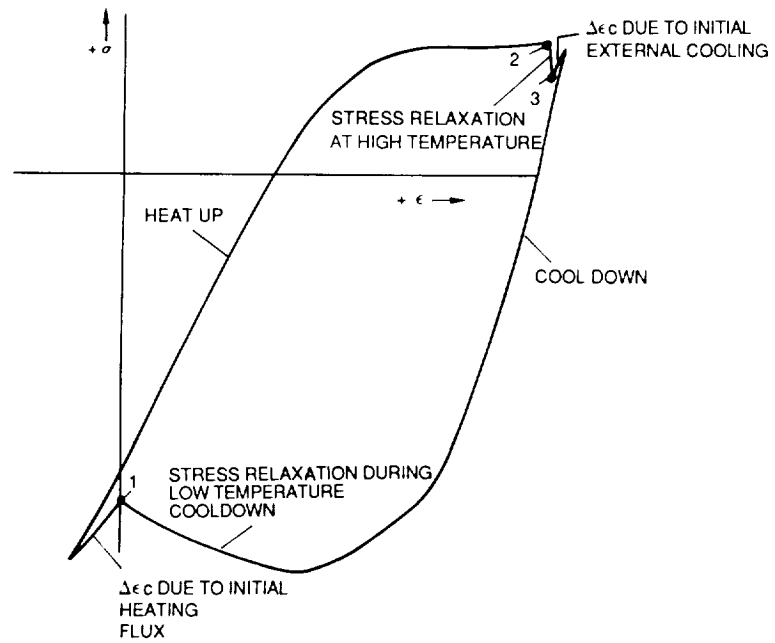


Figure 13 Schematic of Thermally Driven Ceramic Stress Strain Cycle (mature

1  
2  
3  
4  
5  
6  
7  
8  
9  
10  
11  
12  
13  
14  
15  
16  
17  
18  
19  
20  
21  
22  
23  
24  
25  
26  
27  
28  
29  
30  
31  
32  
33  
34  
35  
36  
37  
38  
39  
40  
41  
42  
43  
44  
45  
46  
47  
48  
49  
50  
51  
52  
53  
54  
55  
56  
57  
58  
59  
60  
61  
62  
63  
64  
65  
66  
67  
68  
69  
70  
71  
72  
73  
74  
75  
76  
77  
78  
79  
80  
81  
82  
83  
84  
85  
86  
87  
88  
89  
90  
91  
92  
93  
94  
95  
96  
97  
98  
99  
100